

# Elastica-based strain energy functions for soft biological tissue

K. Garikipati\*, S. Göktepe†& C. Miehe‡

University of Michigan & Universität Stuttgart

## Abstract

Continuum strain energy density functions are developed for soft biological tissues that possess slender, fibrillar components. The treatment is based on the model of an elastica, which is our fine scale model, and is homogenized in a simple fashion to obtain a continuum strain energy density function. Notably, we avoid solving the exact, fourth-order, nonlinear, partial differential equation for deformation of the elastica by resorting to other assumptions, kinematic and energetic, on the response of individual, elastica-like fibrils. The formulation, discussion of responses of different models and comparison with experiment are presented.

## 1 Background

Currently-used strain energy density functions for soft biological tissue have two main origins. Some have been adopted from the rubber elasticity and polymer elasticity literature, and others have functional forms that have been chosen to reproduce the characteristic locking behavior observed in experiments (see Fung, 1993, for a detailed treatment). Among the rubber/polymer elasticity models are micromechanically-derived ones, which mostly incorporate entropic elasticity (see Landau and Lifshitz, 1951, for a discussion). Entropic-elasticity models are suitable for materials in which the uncoiling of long chain molecules under axial force causes a decrease in configurational entropy as fewer configurations become available to the molecule vibrating under its thermal energy (see Ogden, 1997, for detailed treatments of these models). However, it is not clear that the application of entropic elasticity is appropriate for many soft biological tissues such as tendons, ligaments and muscles. As an example, consider the case of tendons, which have a high collagen content. Sun et al. (2002) demonstrated by laser trap experiments that the elasticity of the collagen molecule, which is a triple helix with a diameter of 1.5 nm and a contour length (fully uncoiled length) of approximately 300 nm, is well-represented by the Worm-like Chain Model of Kratky and Porod (1949). However, collagen is not restricted to the form of long chain molecules in the tendon. It forms fibrils of around 300 nm diameter, and lengths of the order of 100s of  $\mu\text{m}$ . These are further ordered into fibers that can run the entire length of tendons (the order of cm). The entire hierarchical structure has extensive crosslinking, including a longitudinal staggering of the collagen molecules that leads to a characteristic banded structure on the scale of a fibril, and a “crimp” with a wavelength of 10 – 50  $\mu\text{m}$ . (Screen et al., 2004; Provenzano and Vanderby, 2006).

---

\* Associate Professor, Department of Mechanical Engineering, and Program in Applied Physics, University of Michigan, Ann Arbor, USA; corresponding author, [krishna@umich.edu](mailto:krishna@umich.edu)

†Research Associate, Institute of Applied Mechanics, Universität Stuttgart, Germany

‡Professor, Dr.-Ing., Institute of Applied Mechanics, Universität Stuttgart, Germany

Given this ordered, hierarchical structure with extensive crosslinking, one must question the use of entropic elasticity. Due to kinematic constraints imposed by the crosslinking it seems unlikely that the collagen molecules are able to sample many configurations via thermal fluctuations. Similar arguments can be made for ligaments and muscles.

Support for this view may be inferred from the experiments of Woo et al. (1987). Strain-controlled cyclic tension tests of canine medial collateral ligaments at temperatures between 2° C and 37° C showed that the area of hysteresis loops on the stress-strain diagram decreased as the temperature of the experiment increased. The use of strain control implies that the decrease in hysteresis was associated with a reduction in initial modulus of the stress-strain curve. In a standard viscoelastic solid, the initial modulus is a material property; in particular, it is independent of viscosity, and therefore not subject to mechanisms of relaxation that may be perceived as a decrease in modulus. This argument leads to the conclusion that, in these experiments, the initial modulus of the stress-strain response was decreasing with an increase in temperature. A decrease in elasticity with increase in temperature is a signature of elastic modulus that arises from variation of internal energy, not of entropic elasticity, which makes the initial modulus increase with temperature (see Treloar, 1975).

One reason for the attractiveness of entropic elasticity models is that they reproduce the experimentally-observed response of soft biological tissue in uniaxial tension shown in Figure 14. We draw attention to the characteristics: a prolonged initial regime with low modulus (the “toe” region), followed by a short nonlinear regime with rapidly-increasing modulus (the “heel” region) and a final high modulus region. We will refer to this as the “characteristic soft tissue response”. However, there are other, non-entropic, models that also reproduce this behavior. It has been typical in the biomechanics literature to use strain energy density functions with mathematical forms that are designed solely to possess this characteristic response (see Fung, 1993). This second class of models is, however, limited by the lack of microstructural bases for the corresponding strain energy functions.

This paper is founded on the recognition that the characteristic locking behavior can be modelled by an internal energy-based, i.e. non-entropic, model of elasticity that accounts for the uncoiling of crimped fibrils with increasing tension. In these models, the characteristic soft tissue response is therefore determined by the elastica-like force versus tip displacement response of the individual fibrils. This consideration leads to a micromechanically-derived strain energy density function for soft tissue, which, as argued above, has the proper basis in internal energy, rather than entropy effects, which are suppressed due to crosslinking.

The realization that characteristic soft tissue response is modelled by the force-displacement response of an elastica—or approximations of it—is hardly new. Diamant et al. (1972) used a planar model of rigid links joined by elastic hinges, which they related to the elastica, to model their observations of stress-stretch behavior of rat tail tendons. In Dale et al. (1972) four kinematic models of crimped fibers were considered: a planar sinusoidal waveform, a helical shape, a zig-zag waveform with hinged apices and a zig-zag with apices that undergo bending to maintain a constant angle while deforming. The change in profile of these waveforms was studied and compared with experiment. Beskos and Jenkins (1975) modelled mammalian tendon as an incompressible composite with a continuous distribution of inextensible fibers with a helical shape. The assumption of inextensibility dominates the response of this model leading to stress locking in uniaxial tension at a finite stretch. The planar assumption was also adopted by Comninou and Yannas (1976), who modelled single collagen fibers as sinusoidal beams. Using the theory of shear deformable beams with linear constitutive relations for axial stretching and bending, but allowing geometric nonlinearities, they obtained a nonlinear stress-strain response of single fibers and extended it to a

composite with uniaxial reinforcement by sinusoidal fibers. In Lanir (1978) a planar model of a beam on an elastic foundation was adopted for the mechanical interaction between collagen (modelled as a beam) and elastin (the elastic foundation). Similar ideas were explored by Kastelic et al. (1980), in whose model crimped collagen fibers were modelled by links that have negligible stiffness until fully extended. The classical theory of elasticas was used by Buckley et al. (1980) to treat the deformation of slender filaments, and the model was solved numerically. Basu and Lardner (1985) also studied the stress-stretch response of sinusoidal beams in elastic matrices, although they did not make the link to fibrous soft tissue. A kinematic chain with finite axial stiffness and torsional springs was used by Stouffer et al. (1985) to represent the uncoiling of crimped fibers, and compared against experiments. More recently, Hurschler et al. (1997) developed a strain energy density function for tendon and ligament with seven parameters including microstructural organization to describe the stress-stretch behavior. The authors also derived simplified versions of their model that were used to fit experimentally-determined, nonlinear stress-stretch curves. Finally, Freed and Doehring (2005) returned to the assumption of a helical structure for collagen fibrils, and using Castigliano's theorem, obtained the force-displacement relationship.

In this communication, we present a very general and powerful procedure for developing the strain energy density function for soft tissue based on the elastica as a model for slender fibrillar structures. To fix ideas, we refer to collagen fibrils. In a notable departure from the body of work cited above, we first obtain the exact, nonlinear, fourth-order elliptic partial differential equation for the quasi-static deformation of the extensible elastica. The underlying kinematics are fully nonlinear and the elastica's strain energy is assumed to be given by quadratic functions of curvature and the Green-Lagrange strain tensor.<sup>1</sup> The difficulty of obtaining analytic solutions of even simpler versions of the governing partial differential equation has been noted by some of the authors cited above. Furthermore, numerical solutions, while possible, will prove both expensive and cumbersome, since our ultimate aim is a strain energy density function for composite soft tissue in which the elastica-like fibrils are the reinforcements at a microscopic scale. For this reason we have examined a few distinct assumptions that make it possible to obtain force-extension solutions. These assumptions are related to the kinematic and energetic behavior of the microscopic collagen fibrils. At the outset we wish to emphasize that these assumptions, in addition to being well-motivated in our view, are most important to this study because they deliver a tractable problem, with only a small number of parameters that are also physically-meaningful. This is a theme that we will return to at several points in the paper. With this approach we have also been able to identify a model that can be made to correspond well with experimental data. A rigorous validation of these assumptions must, however, await *in situ* studies of deforming fibrils.

The organization of the remainder of the paper is as follows: In Section 2 we lay down the fundamental problem of the elastica. The cases of elasticas that are restricted to circular and sinusoidal arcs, and have further constraints of kinematics and energetics imposed upon them, are developed in Sections 3 and 4, respectively. The various models for the deforming elastica are compared against each other, and against experiment, in Section 5. The extension to macroscopic strain energy density functions, from which the tissue stress-stretch response can be obtained, and a basic discussion on convexity appear in Section 6. Closing remarks are made in Section 7.

---

<sup>1</sup>The latter dependence is motivated by the St. Venant-Kirchhoff model, but there is no further significance to this choice. Others are equally admissible and do not imply substantive changes in the outcome.

## 2 The deforming elastica

Consider the elastica, a curve,  $\Gamma \subset \mathbb{R}^3$ , parametrized by its arc length coordinate,  $S$ , in the reference configuration (Figure 1). Points along the curve are identified by position vectors  $\mathbf{X}(S) \in \mathbb{R}^3$ . The tangent at  $S$  is  $\mathbf{T}(S) = d\mathbf{X}/dS$ . Using a Cartesian basis of orthonormal vectors  $\{\mathbf{e}_1, \mathbf{e}_2, \mathbf{e}_3\}$  it is clear that  $dX_I/dS$  is a direction cosine, say  $\cos \alpha_I$ , where  $I = 1, 2, 3$ , and  $\alpha_I$  are the corresponding angles of inclination of  $\mathbf{T}$ . Using the Euclidean norm of a vector,  $\|\mathbf{v}\| = \sqrt{\sum_I v_I^2}$ , it then follows that  $\|\mathbf{T}\| = 1$ . The curvature of  $\Gamma$  is  $\kappa_0 = \|d^2\mathbf{X}/dS^2\|$ . In the deformed configuration,  $\gamma$ , points have position vectors  $\mathbf{x}(S) = \mathbf{X}(S) + \mathbf{u}(S)$ . The tangent vector to  $\Gamma$  is carried to  $\mathbf{t}(S) = d\mathbf{x}/dS$ , and by the chain rule it can be written as

$$\mathbf{t} = \frac{\partial \mathbf{x}}{\partial \mathbf{X}} \frac{d\mathbf{X}}{dS}.$$

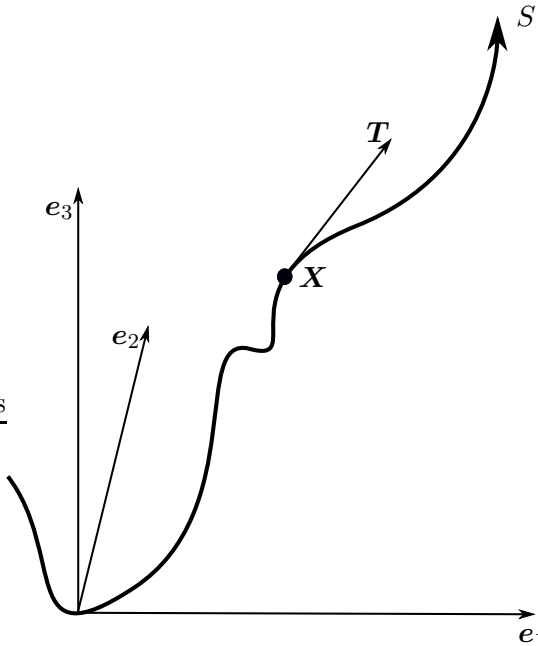


Figure 1: The curve,  $\Gamma \in \mathbb{R}^3$ .

Introducing the deformation gradient tensor,  $\mathbf{F} := \partial\mathbf{x}/\partial\mathbf{X}$ , gives  $\mathbf{t} = \mathbf{FT}$ , from which it follows that  $\|\mathbf{t}\|^2 = \mathbf{T} \cdot \mathbf{CT}$ , where  $\mathbf{C} = \mathbf{F}^T \mathbf{F}$  is the right Cauchy-Green tensor. The stretch along  $S$  will be denoted by  $\lambda := ds/dS = \|\mathbf{t}\|$ , and satisfies  $\lambda > 0$ . As an aside, note that if the arc length in the deformed configuration, say  $s$ , is used to parameterize  $\mathbf{x}$  as  $\mathbf{x}(s)$ , then the tangent with respect to  $\gamma$ , which we will denote by  $\mathbf{t}^\#$ , is given by  $\mathbf{t}^\# = d\mathbf{x}/ds$ , and satisfies  $\|\mathbf{t}^\#\| = 1$ . The curvature of  $\gamma$  is  $\kappa = \|d^2\mathbf{x}/ds^2\|$ , and, clearly, it can be written as  $\kappa = \|d^2\mathbf{x}/\lambda^2 dS^2\|$ .

Motivated by the decoupling of the bending and stretching energies of the classical Euler-Bernoulli beam, we assume that in the present nonlinear setting the strain energy of  $\Gamma$  can also be decomposed into bending and stretching components,  $W(\kappa, \lambda) = K(\kappa) + U(\lambda)$ . The bending stiffness is denoted by  $B$ , the stretching modulus by  $E$ , cross-sectional area by  $A$ , and the reference contour length by  $L$ . This gives

$$K(\kappa) = \int_0^L \frac{1}{2} B(\kappa - \kappa_0)^2 dS, \quad U(\lambda) = \int_0^L \frac{1}{2} EA(\lambda^2 - 1)^2 dS. \quad (1)$$

Observe that  $W(\kappa, \lambda)$ ,  $K(\kappa)$  and  $U(\lambda)$  denote functionals of the corresponding arguments. For simplicity, we will assume that the bending and axial stiffnesses are constant;  $B = \text{const.}$ ,  $EA = \text{const.}$  Also see Section 2.1 in this regard.

The governing partial differential equation for the deformation of the elastica is obtained by imposing stationarity of the following free energy functional, in which the above definitions of curvature and stretch have been exploited:

$$\mathcal{G}[\mathbf{u}] = \int_0^L \left( \frac{1}{2} B \left( \left\| \frac{d^2 \mathbf{x}}{ds^2} \right\| - \kappa_0(S) \right)^2 + \frac{1}{2} EA \left( \left\| \frac{d\mathbf{x}}{dS} \right\|^2 - 1 \right)^2 - \mathbf{q} \cdot \mathbf{u} \right) dS. \quad (2)$$

Note that the strain energy has been incorporated from (1) and  $\mathbf{q}(S)$  is the external force per unit contour length. We have also assumed that the displacement is specified at  $S = \{0, L\}$ :  $\mathbf{u}(0) = \mathbf{0}$  and  $\mathbf{u}(L) = \mathbf{g}$ . Introducing the variations  $\mathbf{x}_\varepsilon = \mathbf{X} + \mathbf{u} + \varepsilon \mathbf{w}$ , where  $\varepsilon \in \mathbb{R}$  and  $\mathbf{w}(S)$  is an arbitrary vector field satisfying  $\mathbf{w}(S) = \mathbf{0}$  at  $S = \{0, L\}$ , the stationarity condition is

$$\frac{d}{d\varepsilon} \mathcal{G}[\mathbf{u}_\varepsilon] \Big|_{\varepsilon=0} = \frac{d}{d\varepsilon} \left( \int_0^L \left( \frac{1}{2} B \left( \left\| \frac{d^2 \mathbf{x}_\varepsilon}{ds^2} \right\| - \kappa_0(S) \right)^2 + \frac{1}{2} EA \left( \left\| \frac{d\mathbf{x}_\varepsilon}{dS} \right\|^2 - 1 \right)^2 - \mathbf{q} \cdot \mathbf{u}_\varepsilon \right) dS \right)_{\varepsilon=0} = 0. \quad (3)$$

Standard variational calculus, the arbitrariness of  $\mathbf{w}$  and  $d\mathbf{w}/dS$ , as well as the homogeneity of  $\mathbf{w}$  at  $S = \{0, L\}$ , yield the following Euler-Lagrange equations:

$$B \frac{d^2}{\lambda d(\lambda dS)} \left( (1 - \kappa_0/\kappa) \frac{d^2 \mathbf{x}}{\lambda d(\lambda dS)} \right) - 2EA \frac{d}{dS} \left( (\lambda^2 - 1) \frac{d\mathbf{x}}{dS} \right) - \mathbf{q} = 0, \quad (4)$$

with the boundary conditions

$$\mathbf{u}(0) = \mathbf{0}, \quad \mathbf{u}(L) = \mathbf{g}, \quad B \left( 1 - \frac{\kappa}{\kappa_0} \right) \frac{d^2 \mathbf{x}}{\lambda d(\lambda dS)} = 0 \text{ at } S = \{0, L\}. \quad (5)$$

Since  $\lambda = \|d\mathbf{x}/dS\|$  and  $\kappa = \|d^2 \mathbf{x}/\lambda^2 dS^2\|$ , Equation (4) possesses complexity beyond that apparent in its form above. In addition to the boundary conditions on  $\mathbf{u}$  at  $\{0, L\}$ , note that the generalized force satisfies homogeneous boundary conditions at  $S = \{0, L\}$  in (5)<sub>3</sub>.<sup>2</sup> Alternate boundary conditions can be used in the above variational procedure.

## 2.1 Simplifying assumptions on kinematics and energetic response of the elastica

The ultimate aim of this work is the development of a macroscopic strain energy density function, where the micromechanics arises from the deformation of the elastica. The *exact* micromechanics of the deforming elastica is obtained by solving the partial differential equation (4) subject to the boundary conditions in (5). Its solution, however, is nontrivial on account of the nonlinearity and

<sup>2</sup>This generalized force is conjugate to  $d\mathbf{w}/dS$  in the Euler-Lagrange equations arising from (3), and therefore admits the interpretation of a moment.

fourth-order form of the partial differential equation. It is desirable to avoid the complexity and expense of solving this equation repeatedly in fine scale computations that will be coarse-grained in some suitable fashion to obtain the strain energy density function and stress at each material point on the macroscopic scale. For this reason, we examine certain assumptions, kinematic and energetic, which simplify the micromechanics.

The kinematic assumption in Section 3 is of an elastica which deforms through a family of circular arcs. In Section 4 it is a family of sinusoidal waveforms. In both sections we also consider two further kinematic assumptions, inextensibility and planar incompressibility, and the assumption of a stationary strain energy. Planar waveforms have been used in many of the studies cited in Section 1, and reported in the experimental studies of Screen et al. (2004) and Provenzano and Vanderby (2006). Helical forms have also been reported in a few cases (see Beskos and Jenkins, 1975; Freed and Doehring, 2005, although even these authors cite at least an equal number of papers that reported planar waveforms). Since there exists some dispute in the literature in this regard, we have chosen the simplicity of planar waveforms. We also note the ease of parametrization of the circular and sinusoidal forms.

The persistence of the initial family of waveforms, and the assumptions of inextensibility or planar incompressibility are, perhaps, the strongest assumptions in this paper. The assumption on persistence of the family of waveforms maintains the ease of parametrization gained by assuming circular arc and sinusoidal initial waveforms. For each of the assumed waveform families (circular arc and sinusoidal) and additional kinematic assumptions (inextensibility and planar incompressibility) we treat the effective elastic parameters,  $B$  and  $E$ , as those measured in an experiment in which the elastica's deformation remains within the waveform family, with the additional kinematic assumptions holding. We note that the effective elastic parameters so measured will be different from those obtained in unconstrained experiments. For simplicity we assume  $B$  and  $E$  to be constant for each combination of waveform family and kinematic assumption. Also note, however, that these parameters will differ in each one of these cases. In each case, we will not solve the unconstrained problem, but will restrict ourselves to the specific waveform family, and additional kinematic assumptions, with effective elastic parameters that are assumed to be obtained from corresponding experiments.

Aside from the implication of these effective elastic parameters, we assume that the distributed forces,  $\mathbf{q}$  in (4), vanish. We will focus on the *external force* that is conjugate to the displacement boundary conditions in (5) in the rest of this paper.

**Remark 1.** The treatment of the kinematics discussed above is in direct analogy with constrained formulations in classical, linearized elasticity, such as the plane strain constraint, and the incompressibility constraint. Consider plane strain: The constraint is assumed to be exactly imposed, and we only consider strains in a three-dimensional subspace of the full, six-dimensional space. Denote the strains and stresses by  $\varepsilon_{ij}$  and  $\sigma_{ij}$ , respectively. Consider a plane strain problem in which the body is loaded by controlling  $\varepsilon_{11}$  while letting  $\sigma_{22}, \sigma_{12} = 0$  and maintaining the plane strain constraint,  $\varepsilon_{33}, \varepsilon_{13}, \varepsilon_{23} = 0$ . Importantly, the effective elastic modulus obtained for the  $\sigma_{11} - \varepsilon_{11}$  response differs from the unconstrained case in which, also,  $\varepsilon_{11}$  is controlled while  $\sigma_{ij} = 0$  for  $i, j \neq 1$ . With Young's modulus  $E$  and Poisson ratio  $\nu$  for an isotropic material, this effective modulus is  $E/(1 - \nu^2)$  in plane strain, while in the unconstrained case it is  $E$ . In plane strain,  $\sigma_{33} \neq 0$  is the Lagrange multiplier enforcing  $\varepsilon_{33} = 0$ , and  $\sigma_{13}, \sigma_{23} = 0$  are the Lagrange multipliers corresponding to  $\varepsilon_{13}, \varepsilon_{23} = 0$ , respectively. It will become apparent in Sections 3–4 that the only loading condition of interest in this paper is exactly analogous to the uniaxial loading discussed in this remark in the plane strain context. The identical arguments, point for point, can be made for the incompressibility constraint,  $\varepsilon_{11} + \varepsilon_{22} + \varepsilon_{33} = 0$ .

### 3 Force-displacement response of an elastica deforming as a circular arc

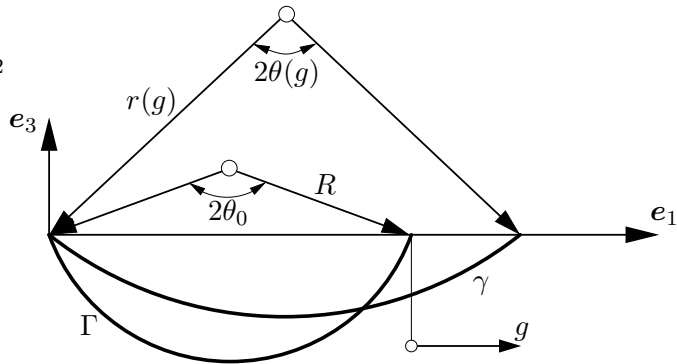


Figure 2: Uncoiling of an elastica shaped as a circular arc.

Consider an elastica with reference configuration,  $\Gamma$ , in the form of an arc of a circle with central angle  $2\theta_0$  and radius  $R$ , as shown in Figure 2. The reference positions of points on  $\Gamma$  are

$$\mathbf{X}(S) = \begin{Bmatrix} R(\sin \theta_0 - \sin(\theta_0 - S/R)) \\ 0 \\ R(\cos \theta_0 - \cos(\theta_0 - S/R)) \end{Bmatrix}, \quad S \in [0, 2R\theta_0] \quad (6)$$

In Sections 3.1–3.3 we explore the effect of further assumptions on this deforming elastica. These are assumptions of (i) inextensibility, (ii) planar incompressibility of the bounding medium, and (iii) stationarity of the strain energy. These cases are not exhaustive. However, the physical interpretations and motivations are transparent.

#### 3.1 The inextensible elastica deforming as a circular arc

The inextensibility assumption is motivated by the relative stiffness in the arcwise direction of the collagen fibril in comparison with the large compliance due to their highly crimped waveform.

Let the point  $S = 2\theta_0 R$  be displaced by the vector  $g\mathbf{e}_1$  while the deformed configuration,  $\gamma$ , maintains the form of a circular arc without extension, i.e.,  $\lambda = 1$ . Then, the tip displacement is restricted to  $0 \leq g \leq 2(\theta_0 - \sin \theta_0)R$ . At a given tip displacement,  $g$ , the central angle of the deformed elastica is  $\theta(g) = \theta_0 R / r(g)$ . The deformed radius,  $r(g)$ , then satisfies the implicit relation

$$r(g) \sin \left( \frac{\theta_0 R}{r(g)} \right) = R \sin \theta_0 + \frac{g}{2} \quad (7)$$

and the positions of points on  $\gamma$  are

$$\mathbf{x}(S) = \begin{Bmatrix} r(g) \left( \sin \theta(g) - \sin \left( \theta(g) - \frac{S}{r(g)} \right) \right) \\ 0 \\ r \left( \cos \theta(g) - \cos \left( \theta(g) - \frac{S}{r(g)} \right) \right) \end{Bmatrix}. \quad (8)$$

From (6) and (8),

$$\frac{d^2\mathbf{X}}{dS^2} = \begin{Bmatrix} \frac{1}{R} \cos\left(\frac{S}{R}\right) \\ 0 \\ \frac{1}{R} \sin\left(\frac{S}{R}\right) \end{Bmatrix}, \quad \frac{d\mathbf{x}}{dS} = \begin{Bmatrix} \cos\left(\theta(g) - \frac{S}{r(g)}\right) \\ 0 \\ -\sin\left(\theta(g) - \frac{S}{r(g)}\right) \end{Bmatrix}, \quad \frac{d^2\mathbf{x}}{dS^2} = \begin{Bmatrix} \frac{1}{r(g)} \sin\left(\theta(g) - \frac{S}{r(g)}\right) \\ 0 \\ \frac{1}{r(g)} \cos\left(\theta(g) - \frac{S}{r(g)}\right) \end{Bmatrix}, \quad (9)$$

from which it follows that  $\kappa_0 = 1/R$ ,  $\kappa = 1/r$  and  $\lambda = 1$ . Note that, for  $g = 2(\theta_0 - \sin \theta_0)R$ ,  $\gamma$  is a straight segment of length  $2\theta_0R$  along  $\mathbf{e}_1$ . Following (1), the strain energy of the elastica can now be written as

$$W(\kappa; g) = \int_0^{2\theta_0R} \frac{1}{2} B (\kappa(g) - \kappa_0)^2 dS, \quad 0 \leq g \leq 2(\theta_0 - \sin \theta_0)R \quad (10)$$

Note that in addition to  $W(\kappa; g)$  being a functional of the field,  $\kappa$ , it is a function of the tip displacement,  $g$ . The force response of the elastica to the tip displacement,  $g$ , is

$$f(\kappa; g) = \frac{\partial W}{\partial g}, \quad 0 \leq g \leq 2(\theta_0 - \sin \theta_0)R \quad (11)$$

Like  $W$ , the force,  $f$ , is a functional of  $\kappa$  and a function of  $g$ . In what follows, the functional character of  $f$  is suppressed since its dependence on  $g$  is of primary interest. Using  $\kappa = \|d^2\mathbf{x}/ds^2\|$ , and equations (9), (7) and (10) we have,

$$f(g) = \frac{B\theta_0R}{r(g)^2} \left( \frac{1}{r(g)} - \frac{1}{R} \right) \frac{1}{\theta \cos \theta - \sin \theta}, \quad 0 \leq g \leq 2(\theta_0 - \sin \theta_0)R. \quad (12)$$

Equation (12) indicates that  $f(g)$  diverges as  $1/r(g) \rightarrow 0$ . Thus the force in a fully uncoiled, inextensible elastica diverges. An extensible elastica, however, develops finite axial tension due to stretching along the tangent as it is uncoiled, and will be considered in the next two sections.

**Remark 2.** We reiterate that the above approach does not involve a formal solution of (4). Instead, it is assumed, *a priori*, that this governing equation is satisfied with the inextensible elastica maintaining the circular arc form.

### 3.2 The extensible elastica deforming as a circular arc and subject to macroscopic, planar incompressibility

Collagen fibrils in soft tissues are surrounded by proteoglycan molecules that bind water. At the levels of stress that the tissue is subject to, the proteoglycan matrix is nearly incompressible. Motivated thus, we consider the waveform of the deforming fibril to be subject to planar incompressibility as a model for full three-dimensional incompressibility (see Remark 5). The elastica deforming as a circular arc in the plane spanned by  $\{\mathbf{e}_1, \mathbf{e}_3\}$  is also subject to invariance of the area of a circumscribing rectangle, even as the rectangle's aspect ratio varies with tip displacement,  $g$ . See Figure 3. The conservation of the area, then, leads us to a closed-form expression for the height,  $a$ , of the current rectangle.

$$A_0 \equiv A \quad \rightsquigarrow \quad a(g) = \frac{2R^2 \sin \theta_0 (1 - \cos \theta_0)}{2R \sin \theta_0 + g}. \quad (13)$$

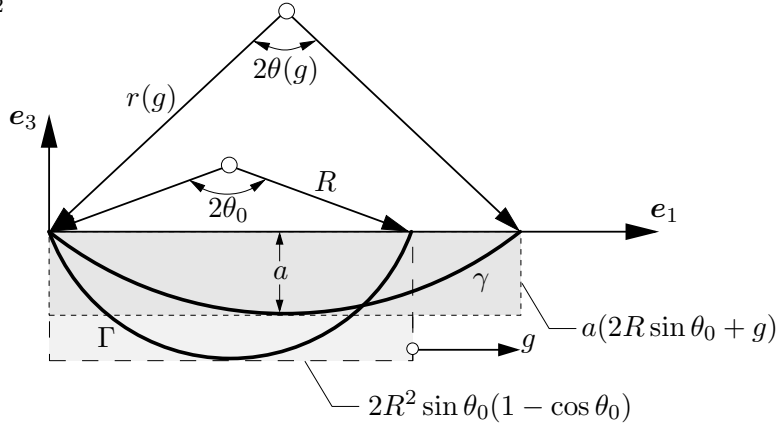


Figure 3: A circular arc elastica surrounded by a two-dimensionally incompressible medium.

With this explicit form of  $a(g)$ , the radius of the deforming elastica can be determined from the geometry of Figure 3 as  $r^2 = (r - a)^2 + (R \sin \theta_0 + g/2)^2$ . This yields

$$r(g) = \frac{1}{2a(g)} \left( (a(g))^2 + \frac{(R^2 \sin \theta_0 (1 - \cos \theta_0))^2}{(a(g))^2} \right). \quad (14)$$

The current curvature  $\kappa(g)$  and stretch  $\lambda(g)$  of the circular arc elastica then immediately follow as

$$\kappa(g) = \frac{1}{r(g)} \quad \text{and} \quad \lambda(g) = \frac{r(g)\theta(g)}{R\theta_0} \quad (15)$$

where the implicit relation (7) is now replaced by

$$\theta(g) = \sin^{-1} \left( \frac{R \sin \theta_0 + g/2}{r(g)} \right). \quad (16)$$

See Figure 3. Inextensibility does not hold:  $\lambda(g) \neq 1$ . Using (15) for  $\kappa(g)$  and  $\lambda(g)$ , and noting that  $\theta$  is a function of  $r(g)$  and  $g$ , we parametrize the strain energy as

$$\overline{W}(r; g) = \int_0^{2\theta_0 R} \frac{1}{2} B \left( \frac{1}{r(g)} - \frac{1}{R} \right)^2 dS + \int_0^{2\theta_0 R} \frac{1}{2} EA \left( \left( \frac{r(g)\theta(g)}{R\theta_0} \right)^2 - 1 \right)^2 dS, \quad (17)$$

where, as previously,  $\overline{W}$  is a functional of  $r$  and a function of  $g$ . The tip force,  $f(g) = \partial \overline{W} / \partial g$ , is

$$\begin{aligned} f(g) &= \theta_0 BR \left( \frac{1}{r} - \frac{1}{R} \right) \left( -\frac{1}{r^2} \right) \left( \frac{3R^2 \sin \theta_0 (1 - \cos \theta_0)}{2a^2} - \frac{a^2}{2R^2 \sin \theta_0 (1 - \cos \theta_0)} \right) \\ &+ EA\lambda(\lambda^2 - 1) \left( 2 \sec \theta + (\theta - \tan \theta) \left( \frac{3R^2 \sin \theta_0 (1 - \cos \theta_0)}{a^2} - \frac{a^2}{R^2 \sin \theta_0 (1 - \cos \theta_0)} \right) \right), \end{aligned} \quad (18)$$

where the derivative formulas  $dr/dg = 3R^2 \sin \theta_0 (1 - \cos \theta_0) / 4a^2 - a^2 / 4R^2 \sin \theta_0 (1 - \cos \theta_0)$ ,  $d\theta/dg = \sec \theta / 2r - \tan \theta dr/dg$  and  $d\lambda/dg = (\frac{1}{2} \sec \theta + (\theta - \tan \theta) dr/dg) / (\theta_0 R)$  have been incorporated.

**Remark 3.** Note that the stretch,  $\lambda$ , defined in (15)<sub>2</sub> is averaged over the reference contour length; i.e., over the circular arc with central angle  $2\theta_0$ . The use of  $\lambda$  in the constitutive relation (17) implies that the axial stiffness,  $EA$ , is also homogenized over the reference contour length.

**Remark 4.** For this case of the circular arc-shaped elastica in a two-dimensionally incompressible medium, it is found that  $\lambda < 1$  for a certain range of *macroscopic stretch*,  $\bar{\lambda} = 1 + g/2R \sin \theta_0$  (see Section 5.1). The incompressibility constraint causes compression of the elastica. If (4) were solved with this macroscopic incompressibility constraint it would manifest itself as buckling. We have not attempted to follow the buckled shape of the elastica. Instead we have solved for the value of  $\theta_0 = \theta_{0\text{cr}}$  such that for all  $\theta_0 < \theta_{0\text{cr}}$  we have  $d\lambda/d\bar{\lambda} > 0$ , ensuring that macroscopic stretch translates to microscopic stretch. This root is  $\theta_{0\text{cr}} \approx 1.342$ . Our numerical studies of the circular arc-shaped elastica in an incompressible medium (Section 5.1) are restricted to  $\theta_0 > \theta_{0\text{cr}}$ .

**Remark 5.**<sup>3</sup> The more physically-realistic condition of volumetric incompressibility leads to the relation

$$V_0 \equiv V \quad \rightsquigarrow \quad a(g) = \sqrt{\frac{2R^3 \sin \theta_0 (1 - \cos \theta_0)^2}{2R \sin \theta_0 + g}}, \quad (19)$$

from which the results follow in the same manner as outlined in this subsection. The results, however, are not qualitatively different between the planar and volumetric incompressibility conditions.

### 3.3 The extensible elastica deforming as a circular arc, and relaxing to a stationary strain energy configuration

Referring to Figure 2, and persisting with the stretch,  $\lambda(g)$ , averaged over the reference contour length as in (15)<sub>2</sub>, the central angle,  $\theta(g)$ , of the deformed elastica as in (16) and  $\kappa(g) = 1/r(g)$ , the strain energy is still given by (17).

For a given tip displacement,  $g$ , corresponding to an applied force,  $f$ , the elastica deforming as a circular arc is now assumed to relax to a deformed radius,  $r(g)$ , at which the strain energy is stationary. The motivation comes from the idea that like long chain bio-molecules, a collagen fibril also attains an equilibrium state with respect to its configuration, in addition to deforming under a tip displacement,  $g$ .

**Remark 6.** As explained in Section 2.1, the force field  $\mathbf{q} = \mathbf{0}$ . Therefore, the corresponding work term does not enter the stationarity calculations. Furthermore, it is assumed that deformation within a subspace of  $\mathbb{R}^3$  for displacements,  $\mathbf{u}$ , manifests in the effective elastic parameters,  $B$  and  $E$  for the elastica deforming as a circular arc. We are interested in stationarity of strain energy *within this subspace of deformation that the elastica is assumed to explore*. That is, the elastica's deformation is allowed to vary only over those configurations allowed while maintaining the circular arc form for this stationarity calculation. Therefore, the work done by Lagrange multipliers that maintain the circular arc shape does not enter the stationarity calculations. With reference to Remark 1, an analogous plane strain calculation would seek stationarity of the strain energy within the strain subspace  $\{\varepsilon_{11}, \varepsilon_{22}, \varepsilon_{12}\}$  while maintaining the plane strain constraint  $\varepsilon_{13}, \varepsilon_{23}, \varepsilon_{33} = 0$ . Therefore, the Lagrange multipliers,  $\sigma_{13}, \sigma_{23}, \sigma_{33}$ , that enforce these constraints do no work, and do not need to be considered in such stationarity calculations. Again, the identical arguments,

---

<sup>3</sup>It was pointed out to us by a reviewer that the condition in this subsection is properly called a “planar incompressibility condition”, which we have now done.

point for point, can be made for a calculation seeking stationarity of the strain energy under the incompressibility constraint; i.e., in the subspace defined by  $\varepsilon_{11} + \varepsilon_{22} + \varepsilon_{33} = 0$ .

The radius,  $r(g)$ , is the solution of the following stationarity condition:

$$\frac{\partial \bar{W}}{\partial r} = 2\theta_0 BR \left( \frac{1}{R} - \frac{1}{r} \right) \frac{1}{r^2} + 4EA\lambda(\lambda^2 - 1)(\theta - \tan \theta) = 0. \quad (20)$$

With the deformed radius thus known, the force is

$$f = \frac{\partial \bar{W}}{\partial g} = 2EA\lambda(\lambda^2 - 1) \sec \theta, \quad (21)$$

since the contribution to  $f$  from the derivatives  $(\partial \bar{W}/\partial r)(dr/dg)$  vanishes by (20).

Note that the extension of the above results (12), (18) and (21) for half-wavelengths to an elastica whose waveform consists of  $n$  such half-wavelengths is straightforward. By symmetry, the force,  $f$ , that results in a total tip displacement of  $g$  corresponds to an extension of  $g/n$  of each half-wavelength, and is obtained from (12), (18) or (21) by substituting  $g$  with  $g/n$ .

## 4 The force-displacement response of a sinusoidal elastica

For the sinusoidal waveform, the reference configuration of the elastica is defined by two shape parameters, the amplitude  $a_0$  and the half-wave length  $l_0$ . See Figure 4. As in Section 3 the

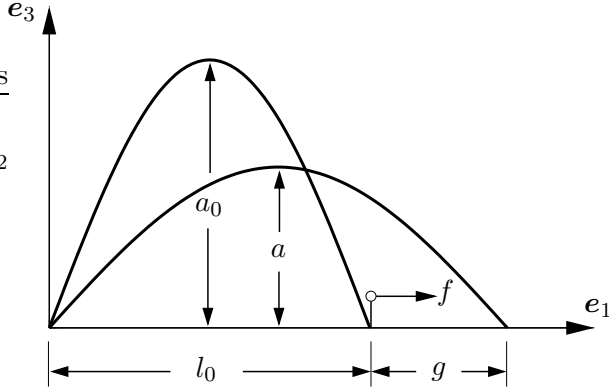


Figure 4: Uncoiling of a sinusoidal elastica.

elastica lies in the plane spanned by  $\{e_1, e_3\}$ . The reference positions of points on the elastica can be expressed by a single parameter,  $t$ , as

$$\mathbf{X}(t) = \begin{Bmatrix} X_1(t) \\ 0 \\ X_3(t) \end{Bmatrix} = \begin{Bmatrix} t \\ 0 \\ a_0 \sin\left(\frac{\pi}{l_0}t\right) \end{Bmatrix} \quad (22)$$

where  $t \in [0, l_0]$ . Analogously, the shape of the deformed elastica can also be formulated in terms of a spatial parameter,  $\tilde{t}$ ,

$$\mathbf{x}(\tilde{t}) = \begin{Bmatrix} x_1(\tilde{t}) \\ 0 \\ x_3(\tilde{t}) \end{Bmatrix} = \begin{Bmatrix} \tilde{t} \\ 0 \\ a \sin\left(\frac{\pi}{l}\tilde{t}\right) \end{Bmatrix} \quad (23)$$

where  $\tilde{t} \in [0, l]$ . The deformed half-wavelength,  $l$ , is determined by the tip displacement  $g$  through the relation  $l := l_0 + g$ . A linear relation therefore exists between  $\tilde{t}$  and  $t$

$$\tilde{t} := t l / l_0 = t (1 + g / l_0) \quad \text{and} \quad \frac{\partial \tilde{t}}{\partial t} = l / l_0 = (1 + g / l_0) . \quad (24)$$

It then follows that the arguments of the Sine functions in (22) and (23) have the same value, i.e.

$$\alpha(t) := \frac{\pi}{l_0} t = \frac{\pi}{l} \tilde{t} . \quad (25)$$

This geometrical description of the problem allows us to introduce the two main kinematic variables, namely the curvature,  $\kappa$ , and the stretch,  $\lambda$ , as functions of derivatives of  $X_3$  and  $x_3$  with respect to the Lagrangian  $t$  and the Eulerian  $\tilde{t}$  parameters, respectively. For the planar reference and current curves parameterized by  $t$  and  $\tilde{t}$ , the general curvature formulas given in Section 2 can be simplified to the forms

$$\kappa_0(t) := \frac{X_3''}{(1 + X_3'^2)^{3/2}} , \quad \kappa(\tilde{t}) := \frac{x_3''}{(1 + x_3'^2)^{3/2}} . \quad (26)$$

The superscript  $(\cdot)'$  in (26) denotes the derivatives

$$\begin{aligned} X_3' &:= \frac{\partial X_3}{\partial t} = a_0 \frac{\pi}{l_0} \cos(\alpha(t)) , \quad X_3'' := \frac{\partial^2 X_3}{\partial t^2} = -a_0 \frac{\pi^2}{l_0^2} \sin(\alpha(t)) , \\ x_3' &:= \frac{\partial x_3}{\partial t} = a \frac{\pi}{l} \cos(\alpha(t)) , \quad x_3'' := \frac{\partial^2 x_3}{\partial t^2} = -a \frac{\pi^2}{l^2} \sin(\alpha(t)) . \end{aligned} \quad (27)$$

The local stretch is obtained as  $\lambda = ds/dS$  where the infinitesimal arc length measures  $dS$ , and  $ds$  are  $dS := \sqrt{dX_1^2 + dX_3^2} = \sqrt{1 + X_3'^2} dt$  and  $ds := \sqrt{dx_1^2 + dx_3^2} = \sqrt{1 + x_3'^2} d\tilde{t}$ , respectively. Then, combining these results with (24)<sub>2</sub> yields the stretch expression

$$\lambda := ds/dS = \frac{\sqrt{1 + x_3'^2}}{\sqrt{1 + X_3'^2}} \frac{l}{l_0} . \quad (28)$$

The basic kinematic variables  $\kappa_0, \kappa(t, g, a(g))$  and  $\lambda(t, g, a(g))$  are thus defined. Note that  $\kappa$  and  $\lambda$  vary pointwise with  $t$  and are parametrized by  $g$  and  $a(g)$ . The total energy of the sinusoidal elastica in the reference configuration is

$$\widetilde{W}(\kappa, \lambda; g, a(g)) = \int_0^{l_0} \frac{1}{2} B(\kappa(t, g, a(g)) - \kappa_0(t))^2 J(t) dt + \int_0^{l_0} \frac{1}{2} EA(\lambda^2(t, g, a(g)) - 1)^2 J(t) dt \quad (29)$$

where  $J(t) := dS/dt = \sqrt{1 + X_3'^2}$ . The tip force  $f(g)$ , being energy-conjugate to the tip displacement  $g$ , is then given by

$$f(g) = \frac{\partial \widetilde{W}(g, a(g))}{\partial g} = \left. \frac{\partial \widetilde{W}(g, a(g))}{\partial g} \right|_a + \left. \frac{\partial \widetilde{W}(g, a(g))}{\partial a} \right|_g \frac{da(g)}{dg} \quad (30)$$

or

$$\begin{aligned} f(g) &= \int_0^{l_0} B(\kappa(t, g, a(g)) - \kappa_0(t)) \left. \frac{\partial \kappa(t, g, a(g))}{\partial g} \right|_t J(t) dt \\ &\quad + \int_0^{l_0} EA(\lambda^2(t, g, a(g)) - 1) \left. \frac{\partial \lambda^2(t, g, a(g))}{\partial g} \right|_t J(t) dt . \end{aligned} \quad (31)$$

where, as previously, the fact that  $f$  and  $\widetilde{W}$  are functionals of  $\kappa$  and  $\lambda$  has been suppressed.

In order to complete the geometric and constitutive description of the deforming sinusoidal elastica,  $a(g)$  must be obtained for each  $g$ . Additional kinematic assumptions are made, as for the elastica deforming as a circular arc. In the case of the sinusoidal elastica, the additional kinematic assumption determines the current amplitude  $a$ . As in Section 3 we consider (i) inextensibility, (ii) a planar incompressible bounding medium, and (iii) stationary strain energy.

#### 4.1 Force-displacement response of an inextensible sinusoidal elastica

The local inextensibility condition requires that  $\lambda := ds/dS = 1$  and thus

$$\lambda^2 - 1 = \frac{1 + x'_3{}^2 l^2}{1 + X'_3{}^2 l_0^2} - 1 = 0. \quad (32)$$

From (27) and (32) we have,

$$a^2 = a_0^2 - \frac{l^2 - l_0^2}{\pi^2 \cos^2(\alpha)}. \quad (33)$$

Clearly, the right hand-side of (33) can be negative, and is unbounded from below in the limit  $\alpha \rightarrow \pi/2$ . Even for positive values of the right hand-side, i.e.  $a^2 > 0$ ,  $a$  as given by (33) varies along the elastica. This indicates that the requirement that  $\lambda = 1$  pointwise along the elastica is inconsistent with maintenance of the sinusoidal shape. It is worth noting that, even physically, it is not clear whether inextensibility should be applied pointwise to model fibrils that are stiff to arcwise extension. It may well prove to be more appropriate to consider inextensibility over a larger length scale. For this reason, we relax this assumption to a weaker one of conservation of the length of the sinusoidal elastica for a given tip displacement  $g$ . We continue to require that  $a = a(g)$  (a function of  $g$  only) and therefore is a parameter for the half wavelength. The weak inextensibility condition gives

$$\int_s ds = \int_S dS \quad \rightsquigarrow \quad \int_0^{l_0} (\lambda(t, g, a) - 1) J(t) dt = 0. \quad (34)$$

This condition defines a non-linear residual that can be considered a function of  $a = a(g)$  for given  $g$ :

$$\mathcal{R}(a) := \int_0^{l_0} (\lambda(t, g, a) - 1) J(t) dt = 0 \quad (35)$$

In order to solve (35) a standard Newton-Raphson iterative scheme must be employed. Recall that this involves the linearization of the residual  $\mathcal{R}(a)$  about  $a = \bar{a}$ ,  $\text{Lin } \mathcal{R}(a)|_{\bar{a}} := \mathcal{R}(\bar{a}) + (\partial \mathcal{R}/\partial a)|_{\bar{a}}(a - \bar{a}) = 0$ , and the solution of this equation for  $a$  to get  $a = \bar{a} - \mathcal{R}(\bar{a})/(\partial \mathcal{R}/\partial a)|_{\bar{a}}$ . For each given value of tip displacement  $g$ , this iterative update scheme is repeated until iterates for  $a$  converge to within a tolerance. Once the value of  $a$  is computed, we proceed with the computation of the tip force  $f$ . To this end, we need the sensitivity of the amplitude  $a(g)$  to the tip displacement  $g$ . It can be calculated by exploiting the implicit form of the residual, now written as  $\mathcal{R}(g, a(g))$  for a general displacement controlled loading process by writing  $d\mathcal{R}(g; a(g))/dg = (\partial \mathcal{R}/\partial g)|_a + (\partial \mathcal{R}/\partial a)(da/dg) = 0$  yielding  $da/dg = -(\partial \mathcal{R}/\partial g)/(\partial \mathcal{R}/\partial a)$ . With this sensitivity in hand, the

integrand in (31) can be computed in a straightforward manner:

$$\begin{aligned}\frac{\partial \kappa}{\partial g} &= \frac{\partial \kappa}{\partial g}\Big|_a + \frac{\partial \kappa}{\partial a}\Big|_g \frac{da}{dg} = \frac{x_3''}{(1+x_3'^2)^{5/2}} \left( \frac{(x_3'^2 - 2)}{l} + \frac{(1-2x_3'^2)}{a} \frac{da}{dg} \right), \\ \frac{\partial \lambda^2}{\partial g} &= \frac{\partial \lambda^2}{\partial g}\Big|_a + \frac{\partial \lambda^2}{\partial a}\Big|_g \frac{da}{dg} = \frac{2l}{l_0^2(1+X_3'^2)} \left( 1 + x_3'^2 \frac{l}{a} \frac{da}{dg} \right).\end{aligned}\quad (36)$$

## 4.2 Force-displacement response of a sinusoidal elastica subject to macroscopic, planar incompressibility

As in Section 3.2 we use planar incompressibility as a model for full, three-dimensional incompressibility. The two-dimensional incompressibility assumption on the surrounding medium (Figure 5) leads to an explicit result for  $a(g)$ .

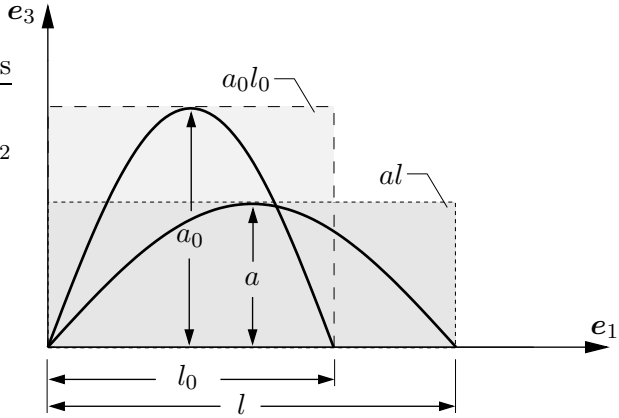


Figure 5: A sinusoidal elastica surrounded by an incompressible medium.

$$a_0 l_0 = a l \quad \rightsquigarrow \quad a(g) = \frac{a_0 l_0}{l} = \frac{a_0 l_0}{l_0 + g}. \quad (37)$$

Once  $a(g)$  is known explicitly in terms of tip displacement  $g$ , the derivatives appearing in (31) can be readily calculated

$$\frac{\partial \kappa}{\partial g} = \frac{3x_3''}{l} \frac{(x_3'^2 - 1)}{(1+x_3'^2)^{5/2}} \quad \text{and} \quad \frac{\partial \lambda^2}{\partial g} = \frac{2l}{l_0^2(1+X_3'^2)}. \quad (38)$$

## 4.3 Force-displacement response of a sinusoidal elastica with stationary strain energy

For the sinusoidal elastica, stationarity of strain energy is imposed with respect to the current amplitude  $a(g)$ , i.e.  $\partial \widetilde{W}(g, a)/\partial a = 0$ . This condition defines a non-linear residual  $\mathcal{R}(a)$

$$\mathcal{R}(a) := \int_0^{l_0} \left( B(\kappa - \kappa_0) \frac{\partial \kappa}{\partial a} + EA(\lambda^2 - 1) \frac{\partial \lambda^2}{\partial a} \right) J(t) dt, \quad (39)$$

which must vanish for a given tip displacement  $g$ . As in Section 4.1 Equation (39) is solved for  $a$  by a Newton-Raphson iterative scheme.

With  $a$  being known the tip force,  $f$ , can be computed. Since the stationary strain energy condition requires that the partial derivative  $\partial \widetilde{W}(g, a)/\partial a$  vanishes, the only terms contributing to the force will be partial derivatives of kinematic variables with respect to the tip displacement  $g$ . That is, it suffices to compute the integrand terms

$$\frac{\partial \kappa}{\partial g} = \frac{x_3''}{l} \frac{(x_3'^2 - 2)}{(1 + x_3'^2)^{5/2}} \quad \text{and} \quad \frac{\partial \lambda^2}{\partial g} = \frac{2l}{l_0^2} \frac{1}{(1 + X_3'^2)}. \quad (40)$$

**Remark 7:** Consider the limiting case in which the tip displacement  $g$  is much larger than the reference half-wavelength  $l_0$ , i.e.  $g/l_0 \gg 1$ , and  $l/l_0 \approx g/l_0 \gg 1$ . The elastica tends toward the limiting shape of a straight segment along  $e_1$ . Owing to the flat shape of the elastica, its spatial slope  $x_3'$  and the curvature  $x_3''$  are small. This implies that the contribution from the bending term to the tip force in both (38)<sub>1</sub> and (40)<sub>1</sub> will be negligible in comparison with the contribution from the axial extension. Furthermore, the vanishing term  $x_3'$  in (38)<sub>2</sub> for large values of the tip displacement  $g$  makes the force terms in (38)<sub>2</sub> and (40)<sub>2</sub> tend toward each other. Then, provided the bending stiffness is not much larger than the axial stiffness, the tip force values for the planar incompressible bounding medium and stationary energy cases approach a common value at large tip displacement values. This is reflected in Figures 12 and 13.

**Remark 8:** Computations with all the models of the sinusoidal elastica discussed in the preceding Sections 4.1– 4.3 require an efficient numerical integration tool both for computing the tip force,  $f$ , and for carrying out the Newton-Raphson iterations. For this purpose, we have employed a set of F77 subroutines, the so-called DCUHRE, providing a double precision integration tool based on adaptive division of the integration domain into subregions. For details of the theory and the implementation of the algorithm, the reader is referred to Berntsen et al. (1991).

## 5 Comparison of shape, kinematic and stationary energy assumptions; validation

We now turn to a comparative study of the force–displacement response of the circular arc and sinusoidal elasticas, with the additional goal of gaining insight to matches between the models and experimental data.

### 5.1 The force-displacement response of circular-arc and sinusoidal elasticas subjected to different kinematic assumptions

We first consider the force–stretch behavior of the circular-arc elastica subject to the two additional kinematic assumptions and the stationary strain energy assumption. To this end, we first relate the micro-tip displacement,  $g$ , and the macro-stretch,  $\bar{\lambda}$ . The displacement between the ends of the elastica is assumed to be dictated by macroscopic deformation in an affine manner. That is, the macro-stretch  $\bar{\lambda}$  is related to the tip displacement  $g$  by  $\bar{\lambda} := 1 + g/(2R \sin \theta_0)$  (see Figure 2). <sup>4</sup> In the studies to follow, the macro stretch will be used as the primary deformation variable controlling the force.

---

<sup>4</sup>For tissues with transverse isotropy, where the collagen fibrils (elasticas) are characterized by end-to-end vectors that are highly aligned, affinity of deformation is a good assumption. The alternative, fibril slippage, will be treated in a separate paper.

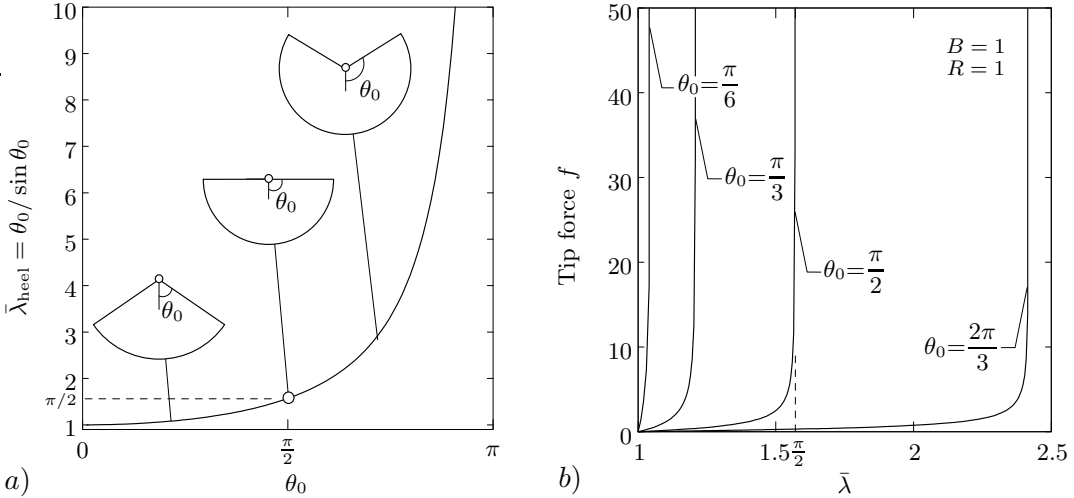


Figure 6: Circular-arc, inextensible elastica. a) Variation of the maximum macro-stretch  $\bar{\lambda}_{\text{heel}} = \theta_0 / \sin \theta_0$  with the initial angle  $\theta_0$ . b) Shift of the maximum value of the attainable macro-stretch  $\bar{\lambda}_{\text{heel}}$  for selected values of the initial angle  $\theta_0 = \frac{\pi}{6}, \frac{\pi}{3}, \frac{\pi}{2}, \frac{2\pi}{3}$ , and for  $B = 1$ ,  $R = 1$ .

For the circular-arc, inextensible elastica, according to (12), the tip force  $f$  diverges as the tip displacement  $g$  approaches the value  $g_{\max} = 2R(\theta_0 - \sin \theta_0)$ . This implies that the maximum value of macro-stretch is  $\bar{\lambda}_{\text{heel}} = \theta_0 / \sin \theta_0$ , as shown also in Figures 6a and 6b. The geometric parameter  $\theta_0$  thus has an unambiguous physical effect. The ordinates of Figure 6a can be obtained as the locking stretch for each value of  $\theta_0$  as shown more transparently in Figure 6b for the  $f-\bar{\lambda}$  response parametrized by  $\theta_0$ . For the circular-arc, inextensible elastica, the shape of the  $f-\bar{\lambda}$  curve depends only on the initial radius  $R$  and the bending stiffness  $B$ . Figures 7a and 7b demonstrate that the larger the initial radius  $R$  or the smaller the bending stiffness  $B$ , the sharper is the transition to divergence in  $f$ . Although the sharpness of the transition can be tuned, the value of the locking stretch remains  $\bar{\lambda}_{\text{heel}} = \theta_0 / \sin \theta_0$ , and the response beyond the heel region is asymptotic to a vertical line at  $\bar{\lambda}_{\text{heel}}$ . Of course, this divergent  $f-\bar{\lambda}$  response is non-physical, and considerably limits the ability to match experiments on different collagenous materials possessing distinct, and non-divergent, responses in the post-heel region.

The variation of the micro-stretch,  $\lambda$ , with macro-stretch,  $\bar{\lambda}$ , for a circular-arc elastica embedded in a planar incompressible medium is depicted in Figure 8a. We draw attention to the compression of the elastica for a regime of deformation characterized by small values of  $\bar{\lambda}$ , and discussed in Remark 4. Following the approach outlined there we have solved for  $\theta_0 = \theta_{0\text{cr}}$  such that for all  $\theta_0 < \theta_{0\text{cr}}$  we have  $d\lambda/d\bar{\lambda} > 0$ . Explicitly we have  $\lambda = \theta(\bar{\lambda})r(\bar{\lambda})/(R\theta_0)$  with  $r(\bar{\lambda}) = R(1 - \cos(\theta_0))/(2\bar{\lambda}) + \bar{\lambda}^3 R \sin^2(\theta_0)/(2(1 - \cos(\theta_0)))$  and  $\theta(\bar{\lambda}) = \sin^{-1}(\bar{\lambda}R \sin \theta_0 / r(\bar{\lambda}))$ . Setting the derivative  $d\lambda/d\bar{\lambda}|_{\bar{\lambda}=1} = 0$  and solving the resulting equation for  $\theta_0$ , we obtained the maximum:  $\theta_0 \leq \theta_{0\text{cr}} \approx 1.342$ . As clearly shown in Figure 8a, for the values of the initial angle  $\theta_0 \leq \theta_{0\text{cr}}$  the compressive regime of micro-stretch is avoided. For this reason our subsequent investigations are restricted to  $\theta_0 \leq \theta_{0\text{cr}}$  for the circular-arc elastica embedded in a planar incompressible medium.

The sensitivity of the tip force,  $f$ , to the axial stiffness,  $EA$ , for  $B = 1$ ,  $R = 1$  and  $\theta_0 = \pi/3$  is depicted in Figure 8b for the circular-arc elastica surrounded by a planar incompressible medium. A decrease in the axial stiffness translates, as expected, to a decrease of the slope. Clearly, the axial stiffness dominates the slope of the  $f-\bar{\lambda}$  curve. In contrast to the inextensible case we observe neither a long toe region nor a distinguishable heel region. Larger values of  $\bar{\lambda}$  are attainable. As the axial stiffness is increased, however, the  $f-\bar{\lambda}$  curve enters the high (but still increasing) slope

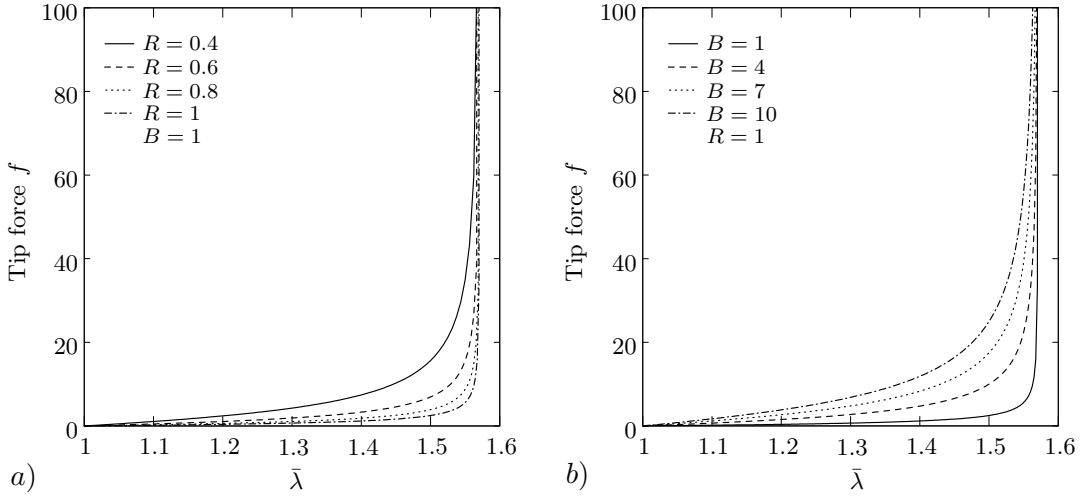


Figure 7: Circular-arc. inextensible elastica. Sensitivity analysis of the  $f - \bar{\lambda}$  curve to a) the variation of initial radius  $R \in [0.4, 1]$  and b) the variation of bending stiffness  $B \in [1, 10]$  for  $\theta_0 = \pi/2$ .

regime about  $\bar{\lambda}_{\text{heel}} = \theta_0 / \sin \theta_0$  without exhibiting much of a toe region. This, of course, limits the use of this model.

The material parameters used for the circular-arc elastica with stationarity of strain energy were the same as for the planar incompressible medium case. As in the planar incompressible case a decrease in axial stiffness has a strong, depressing influence on slope of the  $f - \bar{\lambda}$  response. The elastica can be extended to  $\bar{\lambda} > \theta_0 / \sin \theta_0$ . With an increase in axial stiffness, the  $f - \bar{\lambda}$  curve approaches the behavior of the inextensible circular-arc elastica (see Figure 9). The circular-arc elastica attaining a stationary strain energy possesses a number of favorable properties: The toe region exists and its slope can be tuned by the bending stiffness. The location of the heel region is uniquely determined by the initial angle  $\theta_0$  as  $\bar{\lambda}_{\text{heel}} = \theta_0 / \sin \theta_0$ . The slope of the post-heel region can be adjusted by the axial stiffness  $EA$  as shown in Figure 9. The stationary strain energy assumption with clearly identifiable parameters thus serves as a promising model to match with experimental data.

In Figure 10 we compare all three cases of the circular-arc elastica. Distinct values  $EA = 34, 67, 100$  are assigned to the axial modulus of the planar incompressible and stationary energy elasticas. The  $f - \bar{\lambda}$  curve of the stationary energy case approaches the inextensible one by “rotating” about the heel just below  $\bar{\lambda}_{\text{heel}}$ . However, this occurs with no discernible difference in the curves for  $\lambda$  values smaller than the heel. In case of the elastica surrounded by a planar incompressible medium, however, the stiffening in the  $f - \bar{\lambda}$  behavior is different. Owing to larger values of micro-stretch in the initial stages, the location of the heel shifts to smaller values of  $\bar{\lambda}$ .

In the foregoing parameter study, we solely considered circular-arc elasticas with two kinematic assumptions and the stationary strain energy assumption. In what follows, we present an analogous parameter sensitivity study for the sinusoidal geometry. In contrast to the circular-arc elastica, the reference shape of a sinusoidal elastica is governed by two parameters: the amplitude  $a_0$  and the half-wave length  $l_0$  (see Figure 4). The ratio  $a_0/l_0$ , however, cannot be arbitrarily chosen. According to the results reported by Dale et al. (1972), this ratio is limited to values smaller than 0.1. Accounting for this fact in the studies to follow the ratio has been chosen as  $a_0/l_0 < 0.2$ , which will allow us to consider values slightly larger than the experimental observations. The macro-

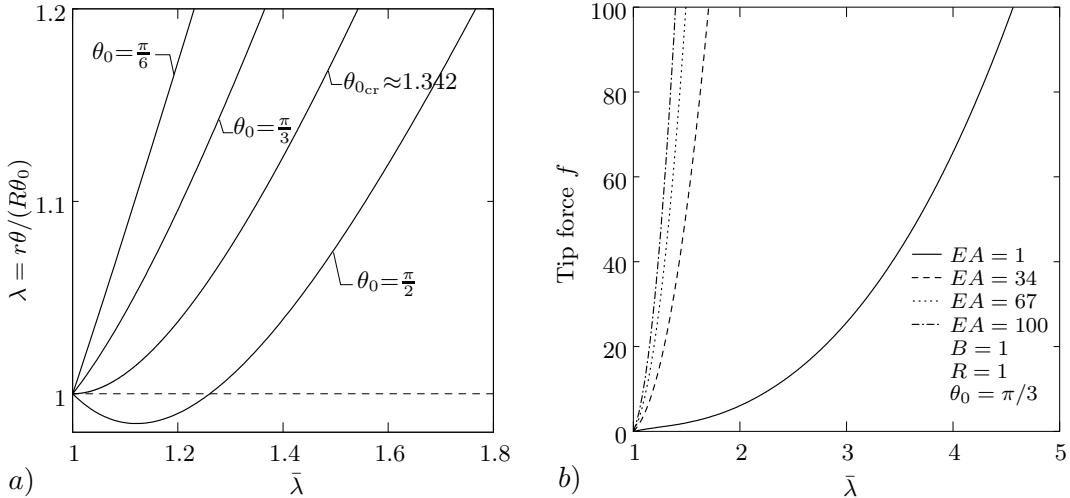


Figure 8: Circular-arc elastica surrounded by a planar incompressible medium. a) Dependence of the micro-stretch  $\lambda$  on the macro-stretch  $\bar{\lambda}$  and the initial angle  $\theta_0$ . b) Sensitivity analysis of the  $f-\bar{\lambda}$  curve to the variation of the axial stiffness  $EA \in [1, 100]$ . curve.

stretch,  $\bar{\lambda}$ , remains the primary deformation measure, and is now related to the tip displacement,  $g$ , by  $\bar{\lambda} = 1 + g/l_0$ .

First, we consider a sinusoidal elastica with the additional global inextensibility assumption given in (34). In Figure 11a the influence of the ratio  $a_0/l_0 \in [0.05, 0.2]$  on the  $f-\bar{\lambda}$  curve is depicted while keeping the material parameters fixed at  $B = 1$  and  $EA = 1$ . This ratio proves crucial in determining the value of stretch at which the heel occurs. The higher the ratio  $a_0/l_0$ , the longer the toe region preceding the heel. In other words, this parameter determines the value of  $\bar{\lambda}$  where the influence of the bending mechanism starts to diminish and the axial extension begins to govern the  $f-\bar{\lambda}$  curve. In order to demonstrate the sensitivity of the  $f-\bar{\lambda}$  curve to the bending stiffness, the ratio of bending stiffness to axial stiffness,  $B/EA$ , is varied from 1 to 4 (Figure 11b). An increase in the ratio  $B/EA$  scales the curve's ordinates ( $f$ -values), and therefore the transition in the heel region becomes more gradual. However, the value of the locking stretch is not influenced by the changes in the ratio  $B/EA$ .

In the last two cases we consider the planar incompressible and stationary energy sinusoidal elasticas. Figures 12a and 13a present the influence of the change in ratio  $a_0/l_0$  on the  $f-\bar{\lambda}$  curves of the respective cases. Like the inextensible case the ratio  $a_0/l_0$  is varied within the interval  $[0.05, 0.2]$  while the value of the ratio  $EA/B$  is kept fixed at 30. Clearly, the  $f-\bar{\lambda}$  curves for the planar incompressible and stationary energy cases do not exhibit a sharp transition to stiffening behavior. This is in contrast with the inextensible case in Figure 11. Variation of the ratio  $a_0/l_0$  does not cause significant change in the shape of the curves.

The sensitivity of the  $f-\bar{\lambda}$  curves for the separate cases to changes in material parameters  $EA$  and  $B$  is presented in Figures 12b and 13b, respectively. The ratio  $EA/B$  varies in the range  $[30, 300]$ . The axial stiffening is clearly reflected in the curves. No striking shape change is observed. We draw attention to the fact that the  $f-\bar{\lambda}$  curves in Figures 12 and 13 for the planar incompressible and stationary energy cases of the sinusoidal elastica are quite similar. The reasons for this similarity have been already outlined in Remark 8.

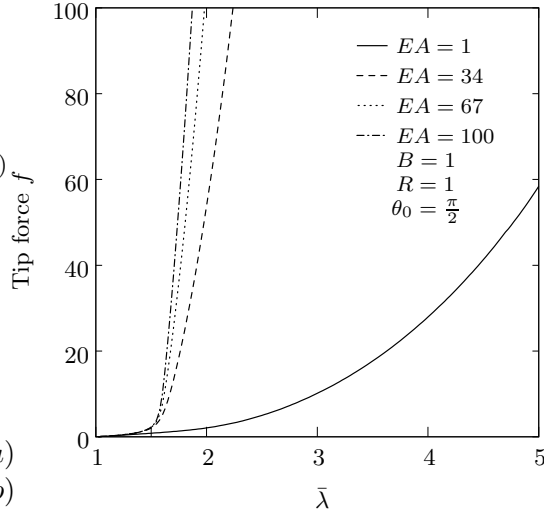


Figure 9: Circular-arc elastica with stationary energy. Sensitivity analysis of the  $f - \bar{\lambda}$  curve to the variation of the axial stiffness  $EA \in [1, 100]$ .

## 5.2 Comparison with experiment

In the preceding section the sensitivities of the  $f - \bar{\lambda}$  curves to geometric and material parameters have been discussed for both the circular-arc and the sinusoidal elasticae subjected to two additional kinematic assumptions, and the stationary strain energy assumption. In this section we carry out a comparison with data reported by Freed and Doehring (2005) (Figure 14). These data correspond to uniaxial extension experiments on five chordae tendineae from porcine mitral valves. They demonstrate a long toe region relative to the maximum stretch in each experiment. At the heel ( $\bar{\lambda}_{\text{heel}} \approx 1.13$ ), the nominal stress–stretch curve stiffens sharply to a larger slope. From the results in Figures 6–13 of the preceding parameter study, it is apparent that this behavior can only be captured either by the inextensible sinusoidal elastica, or the circular-arc elastica attaining a stationary energy state. Figure 14 compares the experiment with these two models with the material parameters given in the caption. Both the sinusoidal and the circular-arc models successfully match the data in the toe region. The inextensible sinusoidal model can also predict the upturning region, but its stiffness beyond the heel region rapidly diverges and fails to match the experimental results. In the case of the circular-arc model, the value of  $\theta_0$  can be analytically determined from the macro-stretch value at the heel. We solve for  $\theta_0$  such that  $\theta_0 / \sin \theta_0 = \bar{\lambda}_{\text{heel}} = 1.13$ . This gives the initial angle  $\theta_0 \approx 4\pi/15$ , and the ratio of the axial and bending stiffness  $EA/B$  can be tuned to match the slopes of the regions just preceding and succeeding the heel region. The initial radius  $R$  is varied to match the sharpness of the slope change at the heel region. The comparison of the stationary strain energy circular-arc elastica and the experimental data clearly illustrates that the proposed model quantitatively captures the experimental data with just a few parameters:  $\theta_0$ ,  $R$ ,  $B$  and  $EA$ , all of which are very well-motivated physically. Clearly, other such experimental data can be matched without difficulty.

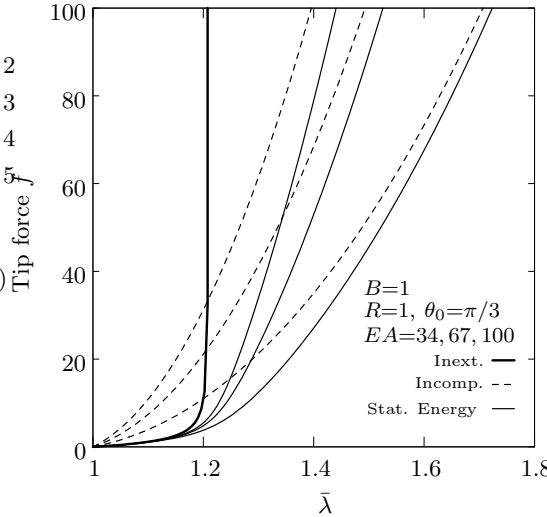


Figure 10: Comparison of circular-arc elasticas subjected to different constraints. In the planar incompressible and stationary strain energy cases, three different values are assigned to the axial stiffness  $EA = 34, 67, 100$ , corresponding to increasingly stiff  $f - \bar{\lambda}$  response.

## 6 Macroscopic material model incorporating the elastica

### 6.1 Continuum strain energy density function at the macroscale

The contribution to the overall strain energy density function due to the collagen fibrils embedded in a nearly incompressible viscous medium is obtained by summing up the free energies of individual elastica-like fibrils,

$$\Psi_{\text{col}} = \frac{N}{A_0 l_0} \widetilde{W}(g). \quad (41)$$

With the unit vector  $\mathbf{e}$  denoting the average orientation of collagen fibrils, the macroscopic stretch in this direction is obtained by  $\bar{\lambda} = |\mathbf{F}\mathbf{e}|$ , where  $\mathbf{F}$  is the deformation gradient tensor. In the context of anisotropic elasticity, especially transverse isotropy, it is common to define structural tensors  $\mathbf{M} := \mathbf{e} \otimes \mathbf{e}$  for the construction of strain energy density functions formulated in terms of additional invariants. The derivatives of these invariants are then used as tensor generators in the stress response functions. In the present case,  $I_4 := \mathbf{C} : \mathbf{M} = \bar{\lambda}^2$  is the relevant invariant ( $\mathbf{C}$  being the right Cauchy-Green tensor). We continue to use an affine relation between the macro-stretch and tip displacement of fibrils, i.e.  $\bar{\lambda} = 1 + g/l_0$ , where  $l_0$  is the half wavelength of a sinusoidal elastica, and  $l_0 = 2R \sin \theta_0$  for a circular-arc elastica. The cross-sectional area of the tissue that contains  $N$  such fibrils is  $A_0$ . With this relation in hand, the contribution to the total second Piola-Kirchhoff stress tensor due to the stretching of collagen fibrils,  $\mathbf{S}^{\text{col}} = 2\partial\Psi_{\text{col}}/\partial\mathbf{C}$ , can be obtained as

$$\mathbf{S}^{\text{col}} = N \frac{f(g)/\bar{\lambda}}{A_0} \mathbf{M} \quad (42)$$

where the results  $\partial g/\partial\bar{\lambda} = l_0$ ,  $2\partial\bar{\lambda}/\partial I_4 = 1/\bar{\lambda}$ ,  $\partial I_4/\partial\mathbf{C} = \mathbf{M}$  and the definition  $f(g) := \partial\widetilde{W}/\partial g$  have been used. Then, the nominal stress tensor  $\mathbf{P}^{\text{col}}$  readily follows from  $\mathbf{P}^{\text{col}} = \mathbf{F}\mathbf{S}^{\text{col}}$ :

$$\mathbf{P}^{\text{col}} = N \frac{f(g)}{A_0} \tilde{\mathbf{e}} \otimes \mathbf{e} \quad (43)$$

where  $\mathbf{F}\mathbf{e} = \bar{\lambda}\tilde{\mathbf{e}}$  and  $|\tilde{\mathbf{e}}| = 1$ .

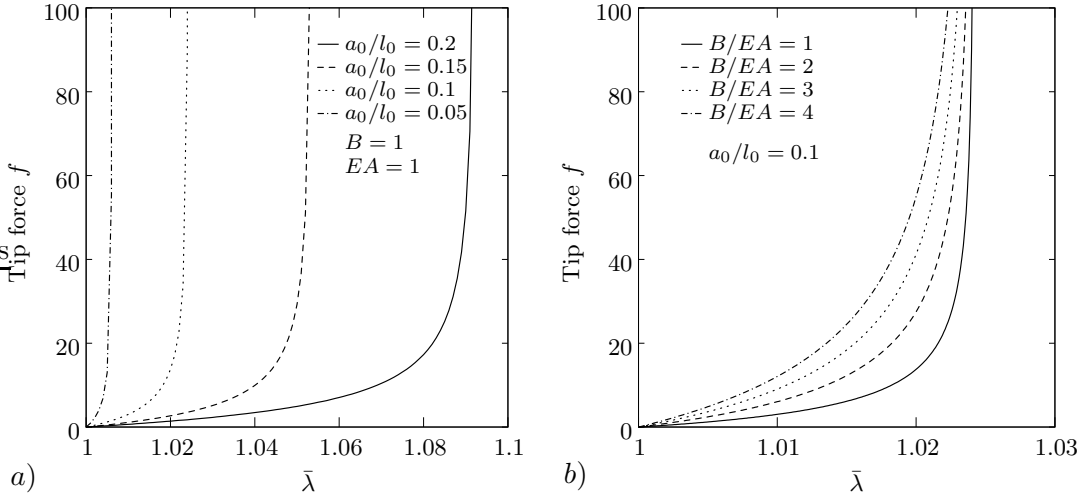


Figure 11: Sinusoidal inextensible elastica. Comparison of the  $f-\bar{\lambda}$  curves for globally inextensible sinusoidal elasticae having different a)  $a_0/l_0$  and b)  $B/EA$  ratios.

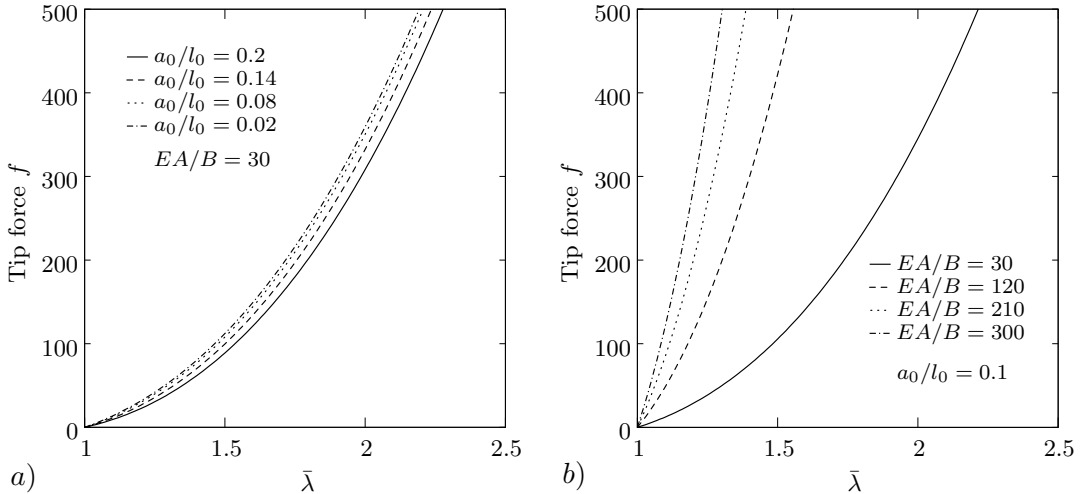


Figure 12: Sinusoidal elastica surrounded by a planar incompressible medium. Comparison of the  $f-\bar{\lambda}$  curves for different a)  $a_0/l_0$  and b)  $EA/B$  ratios.

We now turn our attention to the convexity of the strain energy density  $\Psi_{\text{col}} = \hat{\Psi}_{\text{col}}(I_4)$ , in order to have a basic understanding of its stability properties. The convexity condition demands the positive definiteness of the first elasticity tensor  $\mathbb{A}^{\text{col}}$

$$\mathbf{H} : \mathbb{A}^{\text{col}} : \mathbf{H} \geq 0 \quad \forall \mathbf{H} \in \mathbb{M}^{3 \times 3} \quad \text{and} \quad \mathbb{A}^{\text{col}} := \frac{\partial^2 \hat{\Psi}_{\text{col}}}{\partial \mathbf{F} \partial \mathbf{F}}, \quad (44)$$

where  $\mathbb{M}^{3 \times 3}$  is the space of second-order tensors in  $\mathbb{R}^3$ .

The explicit form of the first elasticity tensor  $\mathbb{A}^{\text{col}}$  can be obtained by the chain rule as

$$\mathbb{A}^{\text{col}} := \hat{\Psi}'_{\text{col}} \frac{\partial^2 I_4}{\partial \mathbf{F} \partial \mathbf{F}} + \hat{\Psi}''_{\text{col}} \frac{\partial I_4}{\partial \mathbf{F}} \otimes \frac{\partial I_4}{\partial \mathbf{F}} \quad (45)$$

where the superscript  $(\cdot)'$  denotes the derivatives with respect to  $I_4$ . The quadratic product of  $\mathbb{A}^{\text{col}}$

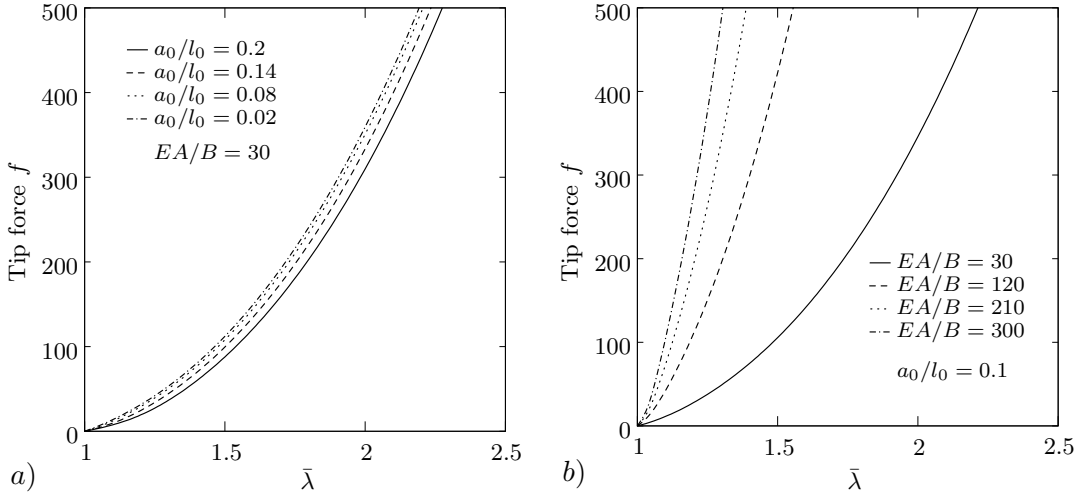


Figure 13: Sinusoidal elastica deforming by attaining a stationary strain energy state. Comparison of the  $f - \bar{\lambda}$  curves for different a)  $a_0/l_0$  and b)  $EA/B$  ratios.

with  $\mathbf{H}$  involves the terms

$$\mathbf{H} : \frac{\partial^2 I_4}{\partial \mathbf{F} \partial \mathbf{F}} : \mathbf{H} = 2\|\mathbf{H}\mathbf{e}\|^2 \geq 0, \quad \left( \frac{\partial I_4}{\partial \mathbf{F}} : \mathbf{H} \right)^2 = (2\mathbf{H}\mathbf{e} \cdot \mathbf{F}\mathbf{e})^2 \geq 0. \quad (46)$$

Note that both terms are non-negative. The local convexity condition (44) of the free energy  $\hat{\Psi}_{\text{col}}$  reduces to

$$2\hat{\Psi}'_{\text{col}} \|\mathbf{H}\mathbf{e}\|^2 + 4\hat{\Psi}''_{\text{col}} (\mathbf{H}\mathbf{e} \cdot \mathbf{F}\mathbf{e})^2 \geq 0. \quad (47)$$

Based on (46), non-negativity of both  $\hat{\Psi}'_{\text{col}}$  and  $\hat{\Psi}''_{\text{col}}$  is sufficient to fulfill the convexity condition (47), though not necessary. The explicit forms of the derivatives are  $\hat{\Psi}'_{\text{col}} = Nf(g)/(2A_0\bar{\lambda})$  and  $\hat{\Psi}''_{\text{col}} = Nl_0(f'(g)l_0 + gf'(g) - f(g))/(4A_0\bar{\lambda}^2(g + l_0))$ . If we assume that collagen fibrils can carry only tensile loads, the positiveness of  $\hat{\Psi}'_{\text{col}}$  is satisfied identically for  $f(g) \geq 0$ . Furthermore, the convexity of  $\hat{\Psi}_{\text{col}}$  with respect to  $g$  ensures that  $f'(g) \geq 0$ . Thus, it is now sufficient to show that the term  $gf'(g) - f(g) \geq 0$  in  $\hat{\Psi}''_{\text{col}}$ . This condition can be obtained starting from the convexity condition for  $f(g)$  with respect to  $g$ , i.e.  $f''(g) \geq 0$ . For positive values of  $g$ , we have  $gf''(g) \geq 0$ . Integration of  $gf''(g) \geq 0$  by parts yields  $\int_0^g gf''(g) = gf'(g)|_0^g - \int_0^g f'(g) \geq 0$ . For  $f(0) = 0$ , we obtain the sought form  $gf'(g) - f(g) \geq 0$ . Therefore, convexity of both the  $\tilde{W}$  and  $f(g) = \partial\tilde{W}/\partial g$  guarantees the local convexity of the macroscopic free energy function  $\hat{\Psi}_{\text{col}}$ .

When  $\hat{\Psi}_{\text{col}}$  is combined by rule-of-mixtures with the strain energy density function of the surrounding matrix medium, the above results completely characterize the influence upon the convexity of the overall composite, leaving open only the question of convexity of the matrix material. However, as pointed out by a reviewer, the actual interaction between the collagen fibrils and matrix involves shearing of the matrix and consideration of the rate of decay of shear fields with distance from a loaded fibril. There is then the possibility of more complex interaction between strain energy of the matrix and of the elastica-like fibrils. The convexity arguments presented here will then have to be refined by further considerations of fibril-matrix interactions.

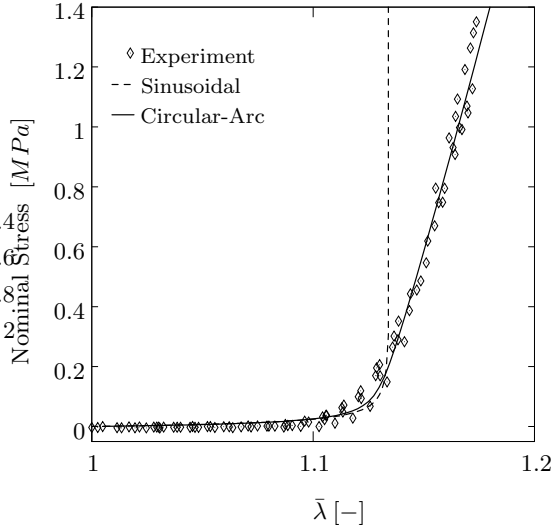


Figure 14: Simulations of experimental data by the inextensible sinusoidal elastica ( $a_0/l_0 = 0.245$ ,  $B/EA = 25 \text{ mm}^{-1}$ ) and the circular-arc elastica attaining a stationary strain energy state ( $R = 0.013 \text{ mm}$ ,  $\theta_0 = 4\pi/15$ ,  $EA/B = 7 \times 10^6 \text{ mm}^{-2}$ ). In the elastica models  $R$ ,  $a_0$  and  $l_0$  were in mm  $B$  in N/mm and  $EA$  in MPa/mm.

## 7 Closing remarks

The primary aim of this paper is a discussion of the characteristic soft tissue response in the context of the elastica-like mechanical behavior of slender fibrillar structures in these tissues. The models are applicable to tendons, skin and the passive response of muscle. While entropic elasticity-based models can also model this characteristic soft tissue response—especially the locking behavior—there are strong physical and physiological reasons to surmise that this is the wrong approach to adopt. A direct solution of the shape and force in a deforming elastica requires the solution of a (“highly”) nonlinear, fourth-order partial differential equation. The simplification used here is that judiciously-chosen additional assumptions on the kinematics and on the energy state can lead to force-deformation response functions for the elastica. This is the central thesis advanced in this paper. Beyond this, the paper is concerned with an enumeration of two families of shapes (circular arcs and sinusoidal half-periods) of the deforming elastica, and three possible additional assumptions: inextensibility, macroscopic planar incompressibility, and stationarity of strain energy. The motivations for each of these additional assumptions are well-founded in a physical sense. Their suitability in matching a set of experimental force-deformation curves has been examined. On the basis of the current limitation to elastic effects, it emerges that the elastica deforming as a circular arc, and maintaining itself in a state of stationary strain energy in each configuration (parametrized by overall elongation) can resolve the experimental data to a high degree of precision.<sup>5</sup> The parameters used are the two stiffnesses—bending and axial, and two geometric parameters that determine the shape of the undeformed elastica. These can be easily determined from mechanical experiments and micrographs, and compared with the values obtained for the best fit. Such an exercise would be a strong validation of these models. We note that the circular-arc elastica with stationary energy matches the experimental data very well in Figure 14 with initial radius  $R = 0.013 \text{ mm}$  ( $13 \mu\text{m}$ ), and initial central angle  $2\theta_0 = 8\pi/15$  ( $96^\circ$ ). This gives a wavelength of  $4R \sin \theta_0 = 38.64 \mu\text{m}$  which seems very reasonable, given that collagen fibrils are typically found to

<sup>5</sup>We have not demonstrated quantitative error measures since no significant physical insight is gained by doing so.

have wavelengths between 10 and 50  $\mu\text{m}$  as in Screen et al. (2004) and Provenzano and Vanderby (2006). The importance of matrix shear lag and its influence on convexity, inelastic effects such as the viscous friction as collagen fibrils move relative to the surrounding proteoglycans, viscoelasticity of the collagen fibrils themselves and proteoglycans, and slippage of fibrils under larger forces, must not be overlooked, however.

It should also be quite clear, that the development here has complete relevance for many types of slender filamentous structures, from carbon nanotubes, through underwater cables to oil pipelines. The class of continuum strain energy density functions so developed in Section 6 is applicable to any composite consisting of mainly unidirectional, elastica-like reinforcing fibers in a matrix.

## References

Basu, A. J., Lardner, T. J., 1985. Deformation of a planar sinusoidal elastic beam. *Journal of Applied Mathematics and Physics* 36, 460–474.

Berntsen, J., Espelid, T. O., Genz, A., 1991. Algorithm 698: DCUHRE: An adaptive multidimensional integration routine for a vector of integrals. *ACM Transactions on Mathematical Software* 17 (4), 452–456.

Beskos, D. E., Jenkins, J. T., 1975. A mechanical model for mammalian tendon. *jam* 42, 755–758.

Buckley, C. P., Lloyd, D. W., Konopasek, M., 1980. On the deformation of slender filaments with planar crimp: theory, numerical solution and applications to tendon collagen and textile materials. *prsla* 372, 33–64.

Comninou, M., Yannas, I. V., 1976. Dependence of stress-strain nonlinearity of connective tissues on the geometry of collagen fibers. *jbm* 9, 427–433.

Dale, W. C., Baer, E., Keller, A., Kohn, R. R., 1972. On the ultrastructure of mammalian tendon. *Experientia* 28, 1293–1295.

Diamant, J., Keller, A., Baer, E., Litt, M., Arridge, R. G. C., 1972. Collagen; ultrastructure and its relation to mechanical properties as a function of ageing. *prslb* 180, 293–315.

Freed, A. D., Doehring, T. C., 2005. Elastic model for crimped collagen fibrils. *ASME Journal of Biomechanical Engineering* 127, 587–593.

Fung, Y. C., 1993. *Biomechanics: Mechanical Properties of Living Tissues*. Springer-Verlag.

Hurschler, C., LoitzRamage, B., Vanderby, R., 1997. A structurally-based stress-stretch relationship for tendon and ligament. *jbme* 119, 392–399.

Kastelic, J., Palley, J., Baer, E., 1980. A structural mechanical model for tendon crimping. *jbm* 13, 887–893.

Kratky, O., Porod, G., 1949. Röntgenuntersuchungen gelöster Fadenmoleküle. *Recueil Trav. Chim* 68, 1106–1122.

Landau, L. D., Lifshitz, E. M., 1951. *A Course on Theoretical Physics, Volume 5, Statistical Physics, Part I*. Butterworth Heinemann (reprint).

Lanir, Y., 1978. Structure-strength relations in mammalian tendon. *Biophys. J.* 24, 541–554.

Ogden, R. W., 1997. Nonlinear Elastic Deformations. Dover Publications, Mineola, N.Y.

Provenzano, P. P., Vanderby, R., 2006. Collagen fibril morphology and organization: Implications for force transmission in ligament and tendon. *Matrix Biology* 25, 71.

Screen, H. R. C., Lee, D. A., Bader, D. L., Shelton, J. C., 2004. An investigation into the effects of the hierarchical structure of tendon fascicles on micromechanical properties. *Proc. Instn. Mech. Engr* 218, 109.

Stouffer, D. C., Butler, D. L., Hosny, D., 1985. The relationship between crimp pattern and mechanical response of human patellar tendon-bone. *jbme* 107, 158–165.

Sun, Y.-L., Luo, Z.-P., Fertala, A., An, K.-N., 2002. Direct quantification of the flexibility of type I collagen monomer. *Biochemical and Biophysical Research Communications* 4295, 382–386.

Treloar, L. R. G., 1975. The physics of rubber elasticity. Oxford Clarendon Press.

Woo, S. L.-Y., Lee, T. Q., Gomez, M. A., Sato, S., Field, F. P., 1987. Temperature-dependent behavior of the canine medial collateral ligament. *J. Bio. Mech. Engrg. Trans ASME* 109, 68.

